Theoretical Characterization of the Reaction Intermediates in a Model of the Nickel−Iron Hydrogenase of *Desulfovibrio gigas*

**Shuqiang Niu,[†] Lisa M. Thomson, and Michael B. Hall***

Contribution from the Department of Chemistry, Texas A&M University, College Station, Texas 77843

Received September 30, 1998. Revised Manuscript Received January 26, 1999

Abstract: The catalytic cycle for H_2 oxidation in [NiFe] *D. gigas* hydrogenase has been investigated through density functional theory (DFT) calculations on a wide variety of redox and protonated structures of the active site model, $(CO)(CN)_2Fe(\mu\text{-}SMe)_2Ni(SMe)_2$. DFT calculations on a series of known $LFe(CO)(CN)(L')^{n-}$ (L = Cp or Cp*, L' = CN, CO, CNCH$_3$; n = 0, 1, 2) complexes are used to calibrate the calculated CO bond distances with the measured IR stretching frequency. By combining this calibration curve with the energy and CO bond distance of the DFT calculations on the active site model and the experimental IR frequencies on the enzyme, the redox states and structures of active site species have been determined: **Ni-B** is a Ni(III)−Fe(II) species, **Ni-SI(a)** is a Ni(II)−Fe(II) species, **Ni-SI(b)** has a protonated terminal sulfur (Ni bound), **Ni-R** is a Ni(II)−Fe(II) dihydrogen complex with H_2 bound at Fe, and **Ni-C** is a Ni(III)−Fe(II) species with an Fe−H−Ni bridge. The latter species returns to **Ni-SI** through a Ni(I)−Fe(II) intermediate, which is potentially observable. Protonation of the Ni bound terminal sulfur results in a folding of the $Fe(\mu\text{-}S)_2Ni$ framework. Dihydrogen activation is more exothermic on the Ni(III) species than on the corresponding Ni(II) or Ni(I) species. Our final set of proposed structures are consistent with IR, EPR, ENDOR, and XAS measurements for these species, and the correlation coefficient between the measured CO frequency in the enzyme and the CO distance calculated for the model species is 0.905.

Introduction

As the central feature of hydrogen metabolism in microorganisms, hydrogenases are of great biotechnological interest.[1] These enzymes catalyze the reversible oxidation of H_2 to protons (reaction 1), which can provide an organism with a source of strong reductants.

$$H_2 \xrightarrow{\text{Hydrogenase}} 2H^+ + 2e^- \qquad (1)$$
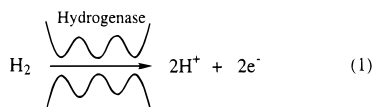
Generally, hydrogenases have been classified into two major classes: iron-only hydrogenases ([Fe]) and nickel−iron ([NiFe]) hydrogenases.[2] In the [NiFe] family, the most studied hydrogenase is that of *Desulfovibrio gigas* since it has been characterized both by the determination of the crystal structure and by many multidisciplinary studies.[1,3] The X-ray crystal structure shows that the [NiFe] hydrogenase of *D. gigas* is an αβ heterodimer with two $[Fe_4S_4]^{2+/1+}$ clusters, one $[Fe_3S_4]^{1+/0}$ cluster, and a binuclear Ni−Fe complex.[3a,b] The Ni−Fe center is the presumptive site of H_2 activation, while the Fe−S clusters serve to transfer electrons.[3a] Electron paramagnetic resonance (EPR) spectroscopy and X-ray absorption spectroscopy (XAS) show that hydrogen activation by [NiFe] hydrogenase takes place in the vicinity of the nickel atom.[4]

The recent experimental reports show that in the catalytic cycle the Ni−Fe complex can be stabilized in six states, called **Ni-A**, **Ni-B**, **Ni-SI**, **Ni-C**, **Ni-R**, and **Ni-SU**.[1,3] Through IR and EPR spectroscopies, the plausible catalytic cycle shown in Scheme 1 has been proposed.[3b−h] For each species in Scheme 1 the labels are also tagged with its CO stretching frequency. The EPR measured results for these species suggest that **Ni-SI**, **Ni-R**, and **Ni-SU** are diamagnetic and that **Ni-A**, **Ni-B**, and **Ni-C** are $S = \frac{1}{2}$ states with the unpaired electron on Ni. Altogether, the experimental work suggests that Ni changes formal oxidation states during the cycle. In addition, the Ni K-edge X-ray absorption spectroscopy (XAS)[3i] suggests that the redox changes of [NiFe] *D. gigas* hydrogenase active site species for **Ni-SI** → **Ni-R** → **Ni-C** do not involve significant electron density changes at the Ni center but the **Ni-A** → **Ni-SI** change does.

† Present address: Environ. Tech. Div., Pacific Northwest National Laboratory, Richland, WA 99352.

(1) Frey, M. *Structure and Bonding*; Springer-Verlag: Berlin, Heidelberg, 1998; Vol. 90, p 97.

(2) (a) Adams, M. W. W. *Biochim. Biophys. Acta* **1990**, *1020*, 115. (b) Przybyla, A. E.; Robbins, J.; Menon, N.; Peck, H. D. *FEMS Microbiol. Rev.* **1992**, *88*, 109. (c) Albracht, S. P. J. *Biochim. Biophys. Acta* **1994**, *1188*, 167.

(3) (a) Volbeda, A.; Charon, M. H.; Pieras, C.; Hatchikian, E. C.; Frey, M.; Fontecilla-Camps, J. C. *Nature* **1995**, *373*, 580. (b) Volbeda, A.; Garcin, E.; Pieras, C.; de Lacey, A. L.; Fernandez, V. M.; Hatchikian, E. C.; Frey, M.; Fontecilla-Camps, J. C. *J. Am. Chem. Soc.* **1996**, *118*, 12989. (c) Dole, F.; Fournel, A.; Magro, V.; Hatchikian, E. C.; Bertrand, P.; Guigliarelli, B. *Biochemistry* **1997**, *36*, 7874. (d) de Lacey, A. L.; Hatchikian, E. C.; Volbeda, A.; Frey, M.; Fontecilla-Camps, J. C.; Fernandez, V. M.; E. C. *J. Am. Chem. Soc.* **1997**, *119*, 7181. (e) Teixeira, M.; Moura, I.; Xavier, A. V.; Huynh, B. H.; Der Vartanian, D. V.; Peck, H. D.; LeGall, J.; Moura, J. J. G. *J. Biol. Chem.* **1985**, *264*, 16435. (f) Roberts, L. M.; Lindahl, P. A. *J. Am. Chem. Soc.* **1995**, *117*, 2565. (g) Happe, R. P.; Roseboom, W.; Piierik, A. J.; Albracht, S. P. J. *Nature* **1997**, *385*, 126. (h) Bagley, K. A.; Duin, E. C.; Roseboom, W.; Albracht, S. P. J.; Woodruff, W. H. *Biochemistry* **1995**, *34*, 5527. (i) Gu, Z.-J.; Dong, J.; Allan, C. B.; Choudhury, S. B.; Franco, R.; Moura, J. J. G.; Moura, I.; LeGall, J.; Przybyla, A. E.; Roseboom, W.; Albracht, S. P. J.; Axley, M. J.; Scott, R. A.; Maroney, M. J. *J. Am. Chem. Soc.* **1996**, *118*, 11155. (j) Montet, Y.; Amara, P.; Volbeda, A.; Vernede, X.; Hatchikian, E. C.; Field, M. J.; Frey, M.; Fontecilla-Camps, J. C. *Nat. Struct. Bio.* **1997**, *4*, 523. (k) Montet, Y.; Garcin, E.; Volbeda, A.; Hatchikian, E. C.; Frey, M.; Fontecilla-Camps, J. C. *Pure Appl. Chem.* **1998**, *70*, 25.

(4) (a) LeGall, J.; Ljungdahl, P.; Moura, I.; Perk, H. D., Jr.; Xavier, A. V.; Moura, J. J. G.; Teixeira, M.; Huynh, B.-H.; Der Vartanian, D. V. *Biochem. Biophys. Res. Commun.* **1982**, *106*, 610. (b) Fernandez, V. M.; Hatchikian, E. C.; Patil, D. S.; Cammack, R. *Biochim. Biophys. Acta* **1986**, *883*, 145.

Scheme 1
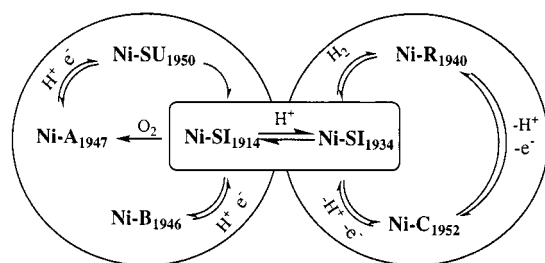
EPR signals: **Ni-A**, **Ni-B**, and **Ni-C**

EPR-silent: **Ni-SU**, **Ni-SI**, and **Ni-R**

Here, using $(CO)(CN)_2Fe(\mu\text{-}SMe)_2Ni(SMe)_2$ as a model, we explore structures for these species, different possible redox states, and levels of protonation by combining experimental data with density functional theory (DFT).[5] Following a brief discussion of the calculations on the organometallic iron site model system,[6] $LFe(CO)(CN)(L')^{n-}$ (L = Cp or Cp*, L′ = CN, CO, CNCH₃; n = 0, 1, 2), we will present several possible candidates for each of the species in the [NiFe] catalytic cycle. Then, by combining the calculated energies, CO bond distances, and spin-density for possible candidate species with experimental results, we arrive at a proposed structural resolution of the intermediate species in the cycle. In developing an enzyme mechanism, it is essential to proceed systematically and identify suitable species for each experimental step, these species should be stable low-energy species and have properties in agreement with the known experimental observations. We hope that this work will lead to a better appreciation of this complicated reaction system. During the preparation of this manuscript, Pavlov et al. published results of DFT calculations on a similar model, $(CO)(CN)_2Fe(\mu\text{-}SH)_2Ni(SH)_2$.[7] However, they assumed that all species were neutral, whereas our results (*vide infra*) suggest that many of the key species involved in the active site are monoanions. Neither of these models includes the protein backbone nor the important hydrogen bonding of the cyanide ligands, both of which will be treated in future studies.

Computational Details

The geometries have been optimized by density functional theory (DFT),[5] specifically with the Becke three-parameter hybrid exchange functional[8] and the Lee−Yang−Parr correlation functional[9] (B3LYP).

Iron and nickel are described by a modified version of the Hay and Wadt basis set with effective core potentials[10a] (ECP). The modifications to the double-ζ basis set were made by Couty and Hall[10b] and give a better representation of the 4p space. The resulting basis set is a (341, 541,41) contraction for iron and nickel, where the 3s and 3p basis functions are left totally contracted but the 4s, 4p, and 3d are split (41), (41), and (41), respectively. For carbon, nitrogen, oxygen, and sulfur, the ECPs and basis sets of Stevens, Basch, and Krauss[11] were

used in double-ζ form. The Dunning−Huzinaga (31) double-ζ basis set was used for the hydrogen atom.[12] In our DFT calculations we replaced cysteines 65, 68, 530, and 533 of the large subunit in the actual [NiFe] *D. gigas* hydrogenase by SCH_3. This simplified model neglects the influence of the bulk protein on the binuclear Ni−Fe structure; this protein structure and the hydrogen bonding to the CN ligands may limit active site folding and ligand rotation. Our calculations show that the folding/unfolding and ligand rotations only lead to small changes in the energy (about 1 kcal/mol) (*vide infra*). Thus, the actual structures found in the enzyme may be somewhat different in detail (Fe−Ni distance, orientation of cysteines), but the key features of the intermediates identified here should be retained.

All DFT calculations were performed with GAUSSIAN94 programs,[13] at the Supercomputer Facility of Texas A&M University and the Department of Chemistry on SGI Powerchallenge, Origin 2000, and Cray J90 computers, and on Silicon Graphic Iris Indigo II and Origin 200 workstations in our laboratory.

Results and Discussion

The CO Bond Lengths and Vibrational Spectra. The relationship between bond length and stretching frequency has had a long history.[14] Recently, based on studies of fast time-resolved infrared (TRIR) spectroscopy, Turner and co-workers showed that there is a relationship between the CO bond length and its energy factored force constants: $r_{CO} = 1.647 - (0.184 \ln k_{CO})$.[15] This relationship can be used for predicting CO bond length changes on electronic excitation of transition metal carbonyls. More recently, Ehlers et al. have presented a study on dissociation energies, vibrational frequencies, and ^{13}C NMR chemical shift of metal hexacarbonyls, $M(CO)_6$ (M = Hf^{2-}, Ta^-, W, Re^+, Os^{2+}, Ir^{3+}, Mo, Tc^+, Ru^{2+}, Cr, Mn^+, Fe^{2+}), using density functional theory.[16] Their results show a strong correlation between the metal charges and both the CO bond distance and the CO stretching frequency.

To examine the relationship between the CO bond length and its vibrational frequency in systems with an Fe−CO bond, similar to that in [NiFe] hydrogenase, we have optimized the model complexes $CpFe(CN)_2(CO)^-$, $CpFe(CN)_2(CO)^{2-}$, $CpFe(CN)(CNCH_3)(CO)$, $CpFe(CN)(CO)_2$, and $Cp^*Fe(CN)_2(CO)^-$ which have been synthesized and studied by Darensbourg et al.[6] The calculations show that an excellent correlation exists between the optimized CO bond lengths and the natural logarithm of the experimental frequencies (Figure 1), where the correlation coefficient is 0.923. One can observe the effect of both redox and ligand changes on the frequency and bond length. Thus, the IR characteristics of the [NiFe] hydrogenase active site should correlate with the calculated CO bond lengths of the correct species. As the electron density on the Ni or the ligands change, the available electron density on the Fe responds and the Fe response shifts the CO bond length and frequency. The redox states of the hydrogenase active site can be characterized by comparing their calculated CO bond lengths with their experimental CO stretching frequencies.

(5) Parr, R. G.; Yang, W. *Density-Functional Theory of Atoms and Molecules*; Oxford University Press: Oxford, 1989.

(6) (a) Darensbourg, D. J.; Reibenspies, J. H.; Lai, C.-H.; Lee, W.-Z.; Darensbourg, M. Y. *J. Am. Chem. Soc.* **1997**, *119*, 7903. (b) Lai, C.-H.; Lee, W.-Z.; Miller, M. L.; Reibenspies, J. H.; Darensbourg, D. J.; Darensbourg, M. Y. *J. Am. Chem. Soc.* **1998**, *120*, 10103. For other model complexes see: Hsu, H.-F.; Koch, S.; Popescu, C. V.; Münck, E. *J. Am. Chem. Soc.* **1997**, *119*, 8371.

(7) Pavlov, M.; Siegbahn, P. E. M.; Blomberg, M. R. A.; Crabtree, R. H. *J. Am. Chem. Soc.* **1998**, *120*, 548.

(8) (a) Becke, A. D. *Phys. Rev.* **1988**, *A38*, 3098. (b) Becke, A. D. *J. Chem. Phys.* **1993**, *98*, 1372. (c) Becke, A. D. *J. Chem. Phys.* **1993**, *98*, 5648.

(9) Lee, C.; Yang, W.; Parr, R. G. *Phys. Rev.* **1988**, *B37*, 785.

(10) (a) Hay, P. J.; Wadt, W. R. *J. Chem. Phys.* **1985**, *82*, 299. (b) Couty, M.; Hall, M. B. *J. Comput. Chem.* **1996**, *17*, 1359.

(11) Stevens, W. J.; Basch, H.; Krauss, M. *J. Chem. Phys.* **1984**, *81*, 6026.

(12) (a) Huzinaga, S. *J. Chem. Phys.* **1965**, *42*, 1293. (b) Dunning, T. H., Jr. *J. Chem. Phys.* **1970**, *53*, 2823.

(13) Frisch, M. J.; Trucks, G. W.; Schlegel, H. B.; Gill, P. M. W.; Johnson, B. G.; Robb, M. A.; Cheeseman, J. R.; Keith, T. A.; Petersson, G. A.; Montgomery, J. A.; Raghavachari, K.; Al-Laham, M. A.; Zakrzewski, V. G.; Ortiz, J. V.; Foresman, J. B.; Cioslowski, J.; Stefanov, B. B.; Nanayakkara, A.; Challacombe, M.; Peng, C. Y.; Ayala, P. Y.; Chen, W.; Wong, M. W.; Andres, J. L.; Replogle, E. S.; Gomperts, R.; Martin, R. L.; Fox, D. J.; Binkley, J. S.; Defrees, D. J.; Baker, J.; Stewart, J. P.; Head-Gordon, M.; Gonzalez, C.; Pople, J. A. Gaussian 94 (Revision D.2); Gaussian, Inc.: Pittsburgh, PA, 1995.

(14) Herzberg, G. *Molecular Spectra and Molecular Structure I. Spectra of Diatomic Molecules*; D. Van Nostrand Company, Inc.: New York, 1957.

(15) Morrison, S. L.; Turner, J. J. *J. Mol. Struct.* **1994**, *39*, 317.

(16) Ehlers, A. W.; Ruiz-Morales, Y.; Baerends, E. J.; Ziegler, T. *Inorg. Chem.* **1997**, *36*, 5031.
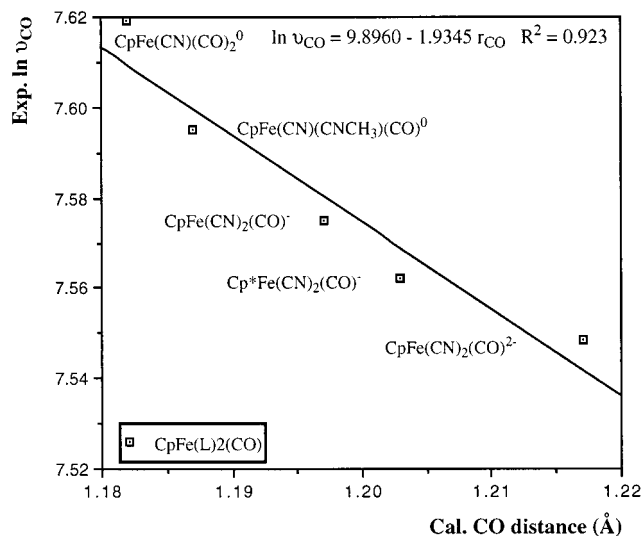
Figure 1. Relationship between the optimized CO bond lengths and experimental CO frequencies of organometallic model complexes $LFe(CO)(CN)(L')^{n-}$ (L = Cp or Cp*, L' = CN, CO, $CNCH_3$; $n = 0$, 1, 2).
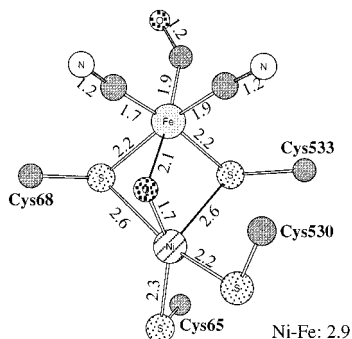

Figure 2. X-ray crystal structure of [NiFe] *D. gigas* hydrogenase. The bridging ligand may be oxo or hydroxo.

The Ni-A and Ni-B Species. The aerobically purified samples of [NiFe] *D. gigas* hydrogenase are characterized by two distinct Ni-EPR signals which are the signatures of two different paramagnetic states of a nickel atom (Ni: $S_1 = {}^1/_2$, Fe: $S_2 = 0$), so-called **Ni-A** and **Ni-B**, respectively.[3c,e] The experimental results also show that **Ni-A** and **Ni-B** have different IR spectra.[3c] The **Ni-A** is catalytically inactive and requires long incubation under H_2 (or a reductant) for activation. The **Ni-B** does not catalyze the activation of H_2, but it may be rapidly converted to the active state by reductants.[3] Accordingly, the two redox states **Ni-A** and **Ni-B** have been termed "unready" and "ready" states, respectively.

The X-ray crystal structure of [NiFe] *D. gigas* hydrogenase shows that the bimetallic [NiFe] center consists of a Ni bound to four cysteines and an Fe bound to two cyanides, a carbon monoxide, and two cysteines, where two cysteines, Cys68 and Cys533, are bridging the Ni atom and the Fe atom (Figure 2).[3a,b] In the oxidized unready species, **Ni-A**, an additional bridge between Fe and Ni is tentatively identified as a μ-oxo or hydroxo ligand. Since the **Ni-B** species can be rapidly converted to the active species, **Ni-SI** (an EPR silent Ni(II)-Fe(II) species), by reductants, **Ni-B** almost certainly corresponds to a Ni(III)−Fe-(II) species.[3c] Candidates for the **Ni-B** species are shown in Scheme 2. There, **2** and **3** arise from protonation on the terminal sulfur atom of **1a** and **2**, respectively. **1b** has been folded to the experimental Ni−Fe distance (2.900 Å) and reoptimized,
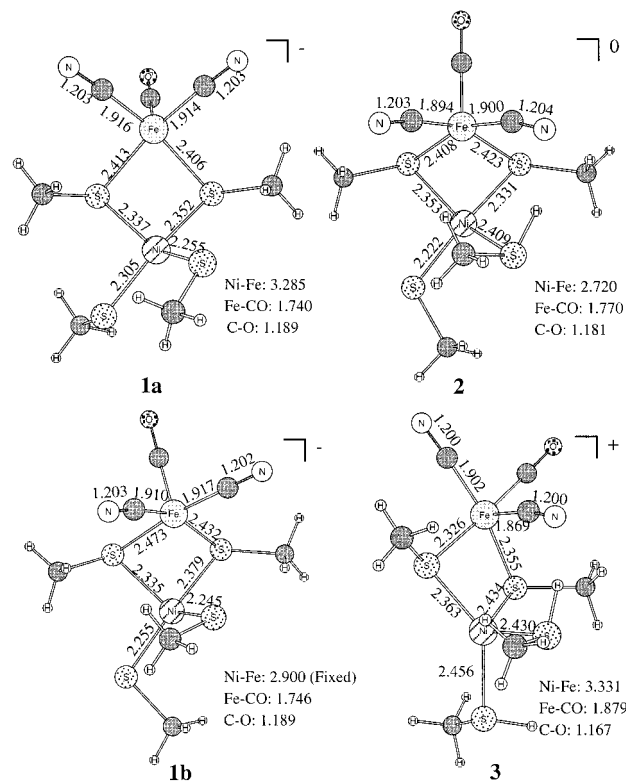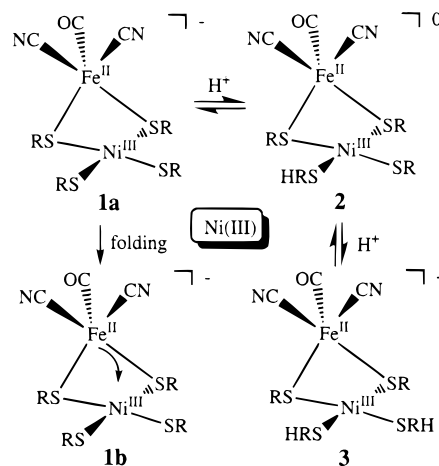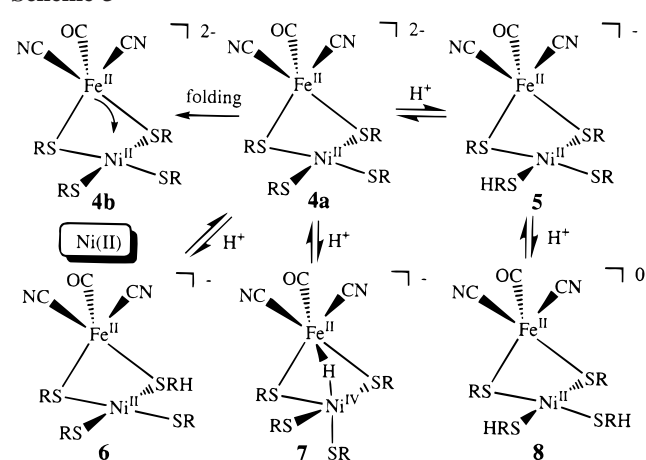
Scheme 2

Figure 3. The B3LYP optimized geometries of the **Ni-B** candidates, **1a**−**3**, and a distorted structure, **1b**.

keeping only this distance fixed. The B3LYP optimized geometries of **1a**−**b**, **2**, and **3** are shown in Figure 3.

In the unprotonated structure **1a**, the distance between the Ni and Fe atoms is 3.285 Å. The five Fe ligands (two cyanides, carbon monoxide, and two bridging cysteines) display square-pyramidal coordination, while the four Ni ligands (two bridging and two terminal cysteines) display distorted square-planar coordination. The twist angle of two terminal cysteines on the Ni relative to the bridging ones is about 28° (dihedral angle between the $Ni(S_{terminal})_2$ plane and the $Ni(S_{bridge})_2$ plane). The spin-density analysis indicates that the unpaired electron is localized on the Ni atom (0.978 e) and the terminal sulfur atom (0.139 e). To examine possible steric effects in the Ni(III) system, we calculated a folded structure **1b**, where the Ni−Fe distance is fixed at 2.900 Å, the experimental value for [NiFe] *D. gigas* hydrogenase. Compared to **1a**, the distortion to **1b** leads to a small change of spin density on the Ni (0.957 e) and

Scheme 3

Figure 4. The B3LYP optimized geometries of the **Ni-SI** candidates, **4a**−**8**, and a distorted structure, **4b**.

practically no change in the CO bond distance. However, in this distortion a cyanide ligand shifts to a bridging position, which leads to a weak stabilizing interaction between the Ni center and the cyanide ligand, such that **1a** and **1b** are essentially isoenergetic. Thus, the protein backbone and the hydrogen bonding to the CN ligands can modulate the actual structure of this species and the CN will probably be restricted from moving to the bridging position shown in **1b** (Figure 3). Upon protonation, **1a** to **2**, the structure folds "naturally" and the Ni−Fe distance of **2** is 0.565 Å shorter than that of **1a**. The spin density on **2** is slightly delocalized from the Ni (0.781 e) to the Fe (0.146 e) atom and the protonated sulfur (0.279 e). Meanwhile, the Fe−CO and C≡O bonds of **2** are longer by 0.03 Å and shorter by 0.008 Å, respectively, than those of **1a**. In contrast to the first protonation, the second protonation, **2** to **3**, opens the Ni−Fe distance by 0.611 Å. As in **2**, the second protonation leads to a longer Fe−CO bond (+0.109 Å) and a shorter C≡O bond (−0.014 Å). Thus, protonation of a terminal (Ni) cysteine, which is favored over a bridging cysteine (vide infra), leads to decrease in the back-donating interaction between the Fe center and the CO ligand.

Two Ni-SI Species, "Active, Oxidized" State. Partial reduction of the enzyme in the **Ni-B** species yields the **Ni-SI** species.[3] The **Ni-SI** species is capable of immediately activating H$_2$, whereas the **Ni-B** species requires a longer time, as indicated by the D$_2$/H$^+$ exchange activity of the two states. Two isoelectronic **Ni-SI** species are observed by IR spectra at different pH values, and both appear to be EPR silent states (*S* = 0 on Ni and Fe).[3c] Since the EPR-silent intermediate **Ni-SI** almost certainly arises from a Ni(II) and Fe(II) species, the possible candidates are shown in Scheme 3. **4b** differs from **4a** because the former is folded with the Ni−Fe distance fixed at 2.900 Å. **5**−**8** differ from **4** in the degree and location of protonation. The B3LYP optimized geometries of **4**−**8** are shown in Figure 4.

In the unprotonated structure **4a**, the distance between the Ni and Fe atoms is 3.321 Å, which is longer by 0.036 Å than that of the unprotonated species, **1a**. The Fe maintains a similar square-pyramidal coordination in both **4a** and **1a**. However, after the reduction from **1a** to **4a**, the square-planar Ni center has its two terminal cysteines twisted by 6° rather than 28°. The Ni−cysteine distances of **4a** are longer than those of **1a**, while the Fe−cysteine distances of **4a** are shorter than those of **1a**. Compared to **1a**, the shorter Fe−CO and longer C≡O distances of **4a** indicate a stronger back-donating interaction. To examine possible steric effects, we calculated a folded structure **4b**, where the Ni−Fe distance is fixed at 2.900 Å, the experimental value
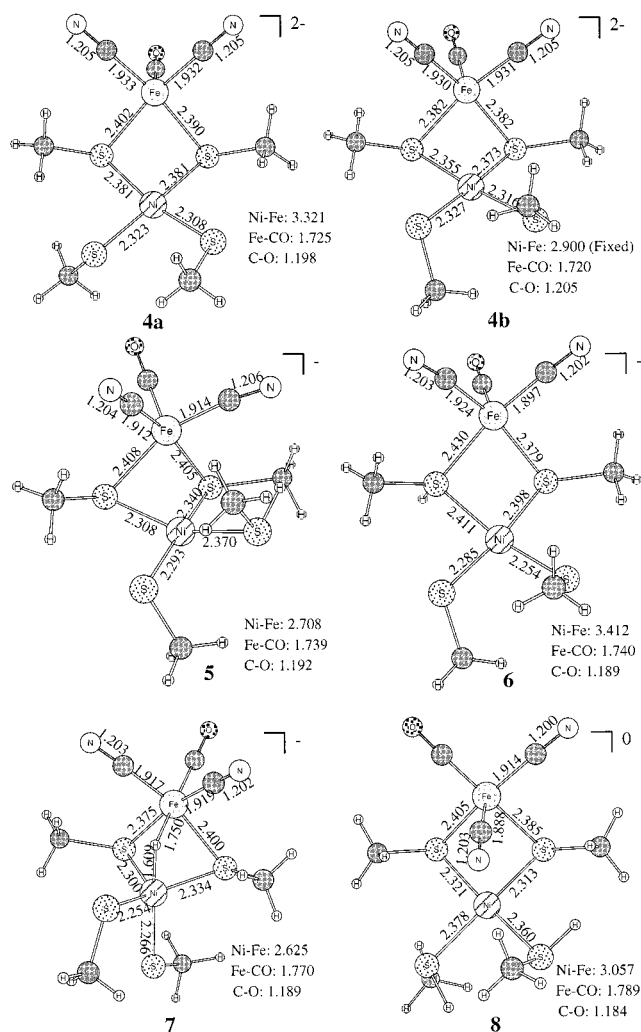
for [NiFe] *D. gigas* hydrogenase. Compared to **4a**, the distances between the metal centers and bridging cysteines of **4b** are all shorter. The changes of the Fe−CO and C≡O from **4a** to **4b** indicate an increase of the back-donating interaction between the Fe center and CO ligand. This distortion to **4b** leads to a destabilization of only 0.90 kcal/mol relative to **4a**.

Like **1a**, a Ni(III) candidate for **Ni-B**, protonation on a terminal sulfur of **4a** leads to a "naturally" folded structure, **5**, where the Ni−Fe distance is shorter by 0.613 Å than that of **4a**. The C≡O distance in **5** reflects a decrease in the back-donating interaction between the Fe center and CO ligand. Protonation of **4a** on a bridging sulfur forming **6** or on the (Ni−Fe) bridging position forming **7** leads to a decrease of the back-donating interaction between the Fe center and the CO with respect to **5**. Compared to the terminally protonated sulfur structure, **5**, the protonated species **6** and **7** are less stable by 19.39 and 25.85 kcal/mol, respectively. Thus, protonation on a terminal sulfur is favored over protonation on a bridging sulfur or in the (Ni−Fe) bridging position, because, in part, the terminal sulfurs have more available lone pairs and bear a more negative charge. Although the second protonation from **5** to **8** changes only slightly the folded structure, it leads to a decrease in the back-donating interaction between the Fe center and the CO ligand of **8** with respect to **5** and it promotes the tendency of a cyanide ligand on the Fe center to bridge. The protonation behavior here is similar to that of the Ni(III) candidates for **Ni-B**.

Scheme 4

Figure 5. The B3LYP optimized geometries of the **Ni-R** candidates, **9**−**13**.
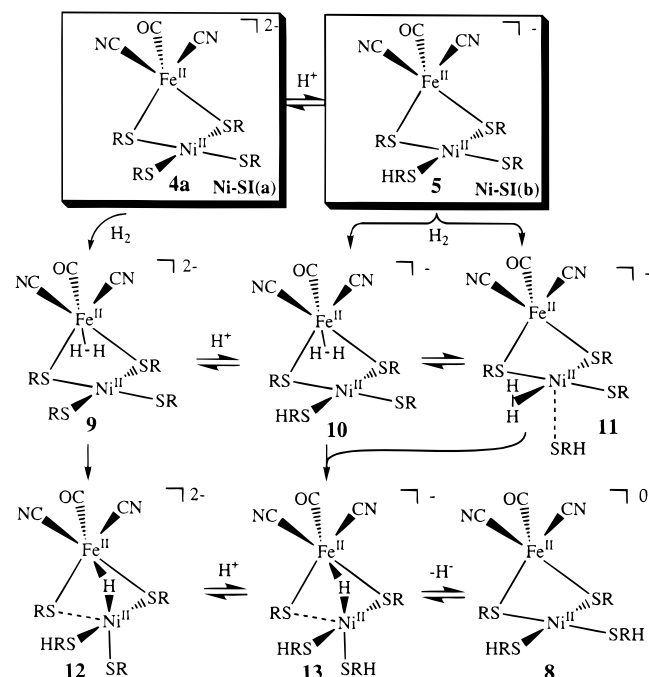
Using both the **Ni-B** and **Ni-SI** results, we can now make structural assignments for **Ni-B** and **Ni-SI**. For **Ni-SI** we have eliminated **6** and **7** based on their energies so the remaining **Ni-SI** candidates are **4a**, **5**, and **8**. For **Ni-B** candidates, **1a**, **2**, and **3**, we can eliminate **3** because its relatively short C≡O bond distance would be incompatible with its measured stretching frequency. If **Ni-B** is **1a** then **Ni-SI(a)** would be **4a** and **Ni-SI(b)** would be **5**. On the other hand, if **Ni-B** is **2** then **Ni-SI(a)** would be **5** and **Ni-SI(b)** would be **8**. Using the least-squares fit (equation) in Figure 1, one can predict the IR spectral changes for the first scenario $\Delta\nu_{1a-4a} = -34$ cm^{-1} and $\Delta\nu_{4a-5} = +22$ cm^{-1}, and for the second $\Delta\nu_{2-5} = -43$ cm^{-1} and $\Delta\nu_{5-8} = +31$ cm^{-1}. The experimental IR spectral data show that the IR spectral changes ($\Delta\nu$) from the **Ni-B** to the **Ni-SI(a)** and from the **Ni-SI(a)** to the **Ni-SI(b)** are -32 and $+20$ cm^{-1}, respectively. Previous work in our laboratory suggests that changes in CO stretching frequencies are predicted by this level of theory to an accuracy of ± 4 cm^{-1}.[17] Thus, the **Ni-B**, **Ni-SI(a)**, and **Ni-SI(b)** species correspond to the dimetal complexes, **1**, **4a**, and **5**, respectively.

Ni-R Species, "Fully Reduced" State. The **Ni-R** species is obtained from **Ni-SI** by reaction with H$_2$. It can oxidize H$_2$ and be oxidized by the [FeS] clusters to form the **Ni-C** species. The experimental spectra show that **Ni-R** is an EPR silent state ($S = 0$ on Ni and Fe).[3] A variety of species have been proposed for **Ni-R**: a Ni^{II}(η^2-H$_2$) complex, a Ni^{II}−H$^-$, a Ni(0) species, and a Ni^{II}(H$^-$)$_2$ complex.[3f] From the **Ni-SI** structures and possible H−H bond activation mechanisms, the **Ni-R** candidates are shown in Scheme 4. **9**−**11** are dihydrogen associated complexes. After the H$_2$ is activated, bridging hydride complexes, such as **12** and **13**, could be formed.

The B3LYP optimized geometries of **9**−**13** are shown in Figure 5. The calculations reveal that the dihydrogen prefers to associate with the Fe center rather than the Ni center, and this association leads to an increase in the Ni−Fe distance with respect to that in **Ni-SI**. In the octahedral Fe(η^2-H$_2$) complexes, **9** and **10**, the H−H bond distances are longer by about 0.02 Å than that calculated for free H$_2$. The H$_2$ association with **4a**
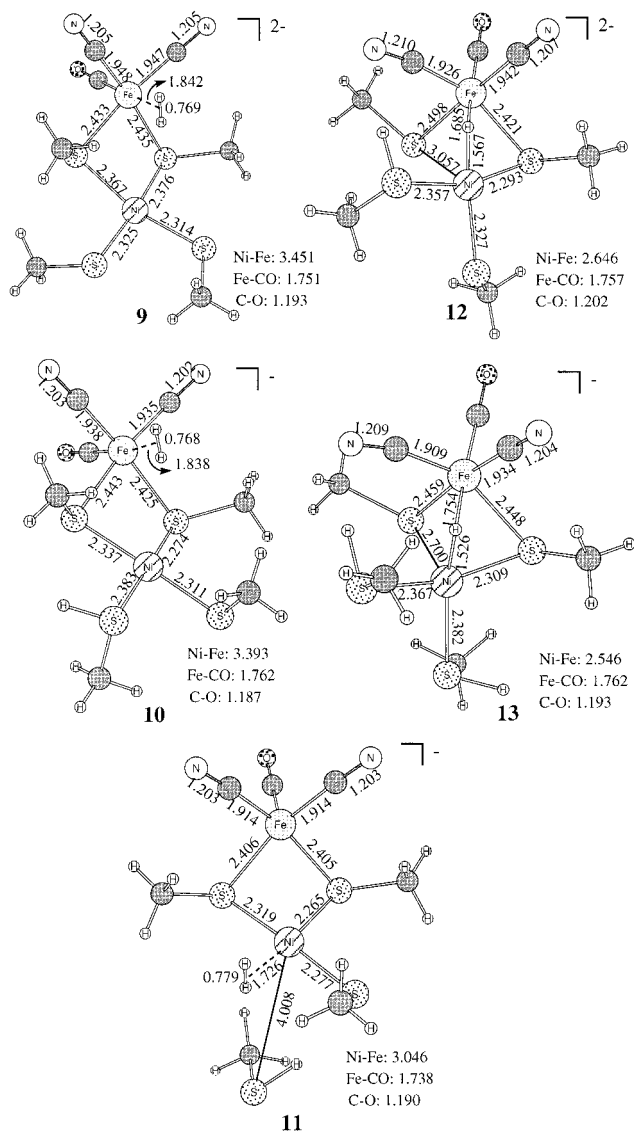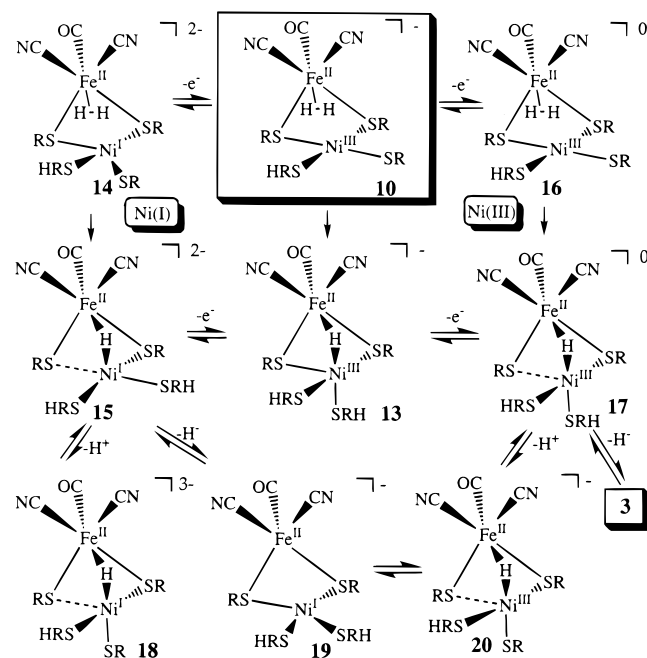
(17) Zaric, S.; Hall, M. B. *J. Phys. Chem. A* **1998**, *102*, 1963.

(**Ni-SI(a)**) and **5** (**Ni-SI(b)**) only leads to a small increase in stability (-4.2 and -0.4 kcal/mol) because of the "unfolding" distortion from **Ni-SI** to **9** and **10**. H$_2$ association with **Ni-SI(b)** could yield a Ni(η^2-H$_2$) complex, such as **11**. However, the H$_2$ association with the Ni center from **Ni-SI(b)** to **11** destabilizes the system by 6.23 kcal/mol and the protonated cysteine−Ni bond breaks in order to maintain the low-spin d^8 Ni square-planar structure.

The bridging hydride complexes, **12** and **13**, show similar structural features: a shorter Ni···Fe distance, an octahedral Fe center, and a square-pyramidal Ni center with a long apical Ni···S distance. Compared to **12**, the protonation of **13** leads to a shorter distance between Ni and the apically bridged cysteine ligand, resulting in a decrease of the back-bonding interaction between Fe and the CO ligand. Since the dihydrogen activation reactions from **9** to **12** and from **10** to **13** are endothermic by 16.7 and 16.9 kcal/mol, respectively, it is debatable that the dihydrogen activation occurs by either of these steps. On the other hand, from the CO experimental vibrational frequency and the calculated bond CO length of **5** (**Ni-SI(b)**), one would conclude that the **Ni-R** species should have a weaker back-bonding interaction between Fe and CO and a shorter C≡O bond (<1.192 Å). Thus, the most likely candidate for the **Ni-R**

Scheme 5

Figure 6. The B3LYP optimized geometries of the **Ni-C** candidates with a Ni(I) center, **14**, **15**, **18**, and **19**. The Ni−terminal-cysteine distances of **14**, **15**, and **18** are fixed at the distance of the corresponding Ni(II) species, **10**, **13**, and **12**, respectively. Forcing the terminal cysteines, which was dissociating from the Ni, caused a symmetric hydrogen bond to form **18**.

species is the dihydrogen associated complex **10** (1.187 Å) rather than **9** (1.193 Å).[18]

Although an η^2-H$_2$ bound to Fe has not been a widely touted suggestion, a low-spin d^6 metal and a ligand mix of soft donors and π acceptors are characteristic requirements for stabilizing a dihydrogen complex.[19,20] The Fe is perfectly configured to make the initial capture of the H$_2$ as it diffuses to the [NiFe] site.[3j,k] The presence of Fe−(η^2-H$_2$) here is also consistent with the existence of iron-only hydrogenases.

Ni-C Species, "Active" State. The **Ni-C** species can be obtained by reducing the **Ni-SI** form or oxidizing the **Ni-R** form.[3] EPR studies show that the **Ni-C** signal arises from paramagnetic states on the nickel (Ni: $S_1 = 1/2$, Fe: $S_2 = 0$), which may correspond to either Ni^{3+} or Ni^{1+}.[3c] In the catalytic cycle **Ni-C** seems to be the only paramagnetic intermediate and it also appears to be a photolabile hydrogenic species (H$^+$, H$^-$, or H$_2$). **Ni-C** has been proposed to be a Ni(III) species, Ni^{III}−H$^-$, a Ni^{III}(η^2-H$_2$) complex, a protonated Ni(I) species, a Ni^{I}−H$^-$, a Ni^{I}(η^2-H$_2$) complex, and a Ni(II) species with a redox-active ligand radical.[3f] By following the **Ni-SI** and **Ni-R** structures and the H−H bond activation mechanism, our proposed **Ni-C** candidates are shown in Scheme 5. As mentioned above, the dihydrogen activation by the Ni(II) species from **10** to **13** is endothermic by about 17 kcal/mol. Here, the dihydrogen activation by the Ni(I) species, **14** to **15**, and Ni(III) species, **16** to **17**, will be investigated. The species **18**, **19**, **20**, and **3** are H$^+$ and H$^-$ transfer derivatives of **15** and **17**, respectively, just as **12** and **8** were similar transfer derivatives of **13**.

We have carried out the B3LYP optimization along the dihydrogen activation pathways. Although species **14** shows similar structural features to **9** and **10**, where the dihydrogen associates primarily with the Fe center, the Ni center tends toward tetrahedral coordination, as the Ni−S bond between Ni and the protonated cysteine leaves during geometry optimization. Similar phenomena occur in the bridging hydride species **15** and **18**, where (i) the protonated cysteine breaks away from the Ni center, (ii) the Ni center tends toward the tetrahedral structure, and in addition (iii) the structures are clearly folded. Species **19** retains these structural features but the Ni−S bond between Ni and the protonated cysteine does not leave. To help understand the effect of reduction on species **10**, **13**, and **12** we have reoptimized the geometries of **14**, **15**, and **18**, where the Ni−S distances between Ni and the terminal cysteine ligands are fixed at the distance of the corresponding Ni(II) species, **10**, **13**, and **12**, respectively. The B3LYP optimized geometries of **14**, **15**, **18**, and **19** are shown in Figure 6. Compared to the **Ni-B** species, **1a**, species **14**, **15**, **18**, and **19** all have longer CO distances (1.196−1.212 Å) opposite to the trend expected from the **Ni-C** stretching frequency. Furthermore, as in the dihydrogen bond activation by the Ni(II) species (**10** to **13**), the H−H bond activation by the Ni(I) species (**14** to **15**) is endothermic by about 27 kcal/mol. Thus, the Ni(I) species **14**, **15**, **18** and **19** can be ruled out as **Ni-C** candidates.

The B3LYP optimized geometries of the Ni(III) species, **16**, **17**, and **20**, are shown in Figure 7. Species **16** shows similar structural features to those of **9** and **10**, where the dihydrogen associates with the Fe center and the Ni center maintains a square-planar structure. The bridging hydride complexes, **17** and **20**, show a square-pyramidal Ni center, where the two terminal cysteine ligands, a bridging cysteine ligand, and the hydride ligand occupy the equatorial positions and a bridging cysteine ligand with a longer Ni−S bond occupies the axial position. Since the H−H bond activation reaction by the Ni(III) species

(18) According to the linear correlation for r_{CO} vs ln ν_{CO} in Figure 8, the expected B3LYP CO bond distance for **Ni-R** should be 1.189 Å.

(19) (a) Lin, Z.-Y.; Hall, M. B. *Coord. Chem. Rev.* **1994**, *135/136*, 845. (b) Lin, Z.-Y.; Hall, M. B. *Inorg. Chem.* **1992**, *31*, 4262.

(20) (a) Kubas, G. J. *Acc. Chem. Res.* **1988**, *21*, 120. (b) Gilbert, S.; Knorr, M.; Mock, S.; Schubert, U. *J. Organomet. Chem.* **1994**, *480*, 241. (c) Eckert, J.; Albinati, A.; White, R. P.; Bianchini, C.; Peruzzini, M. *Inorg. Chem.* **1992**, *31*, 4241. (d) Li, Z.-W.; Yeh, A.; Taube, H. *Inorg. Chem.* **1994**, *33*, 2874. (e) Perthuisot, C.; Fan, M.-X.; Jones, W. D. *Organometallics* **1992**, *11*, 3622. (f) Albertin, G.; Antoniutis, S.; Delministro, E.; Bordignon, E. *J. Chem. Soc., Dalton Trans.* **1992**, *22*, 3203. (g) Eckert, J.; Kubas, G. J. *J. Phys. Chem.* **1993**, *97*, 2378. (h) Kubas, G. J.; Burns, C. J.; Eckert, J.; Johnson, S. W.; Larson, A. C.; Vergmini, P. J.; Unkefer, C. J.; Khalsa, G. R. K.; Jackson, S. A.; Eisenstein, O. *J. Am. Chem. Soc.* **1993**, *115*, 569.
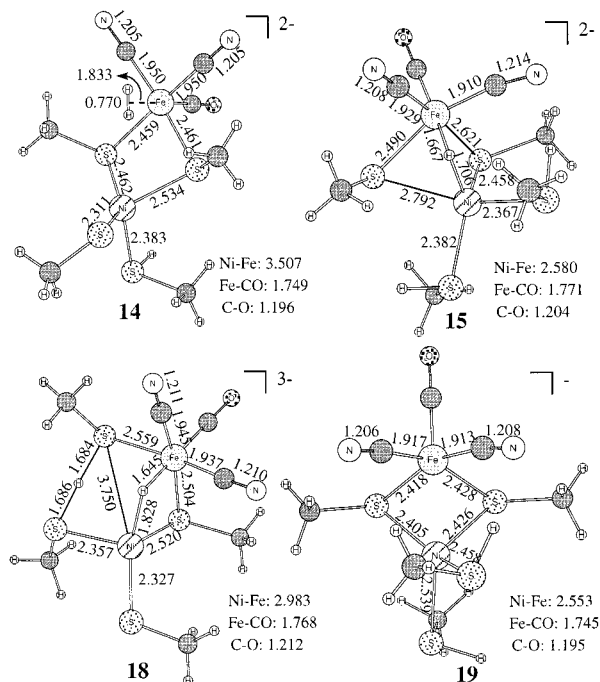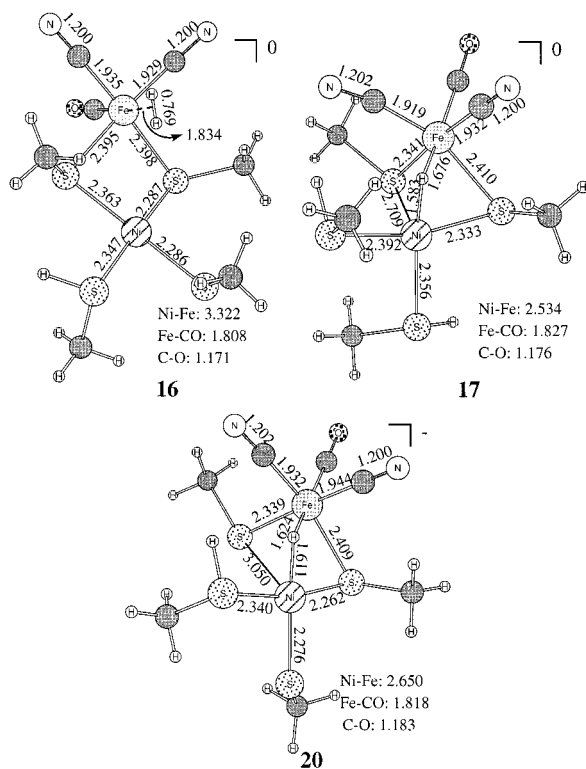
Figure 7. The B3LYP optimized geometries of the **Ni-C** candidates with a Ni(III) center, **16**, **17**, and **20**.

Figure 8. Relationship between the optimized CO bond lengths and experimental frequencies of the intermediates of the [NiFe] hydrogenase.

Table 1. Calculated CO Bond Distances (Å) of Possible Species in the Active Site of [NiFe] Hydrogenase

	$[Ni-Fe]^n$	$[Ni-Fe]^n + H^+$	$[Ni-Fe]^n + 2H^+$	$[Ni-Fe]^n + 3H^+$
$[Ni-Fe]^-$	**1** $(1.189)^a$	**2** (1.181)	**3** (1.170)	
$[Ni-Fe]^{2-}$	**4a** (1.198)	**5** (1.192)	**8** (1.184)	**13** (1.193)
		6 (1.189)		
		7 (1.189)		
$[Ni-Fe]^{3-}$	**21** $(1.227)^b$	**22** $(1.203)^b$	**19** (1.195)	**16** (1.171)
			20 (1.183)	**17** (1.176)
$[Ni-Fe]^{4-}$			**9** (1.193)	**10** (1.187)
			12 (1.202)	**11** (1.190)
			24 $(1.210)^b$	
$[Ni-Fe]^{5-}$			**18** (1.212)	**14** (1.196)
			23 $(1.201)^b$	**15** (1.204)

^{a} The underlined species correspond to the observed [Ni−Fe] species: **1** = Ni-B, **4a** = Ni-SI(a), **5** = Ni-SI(b), **10** = Ni-R, and **20** = Ni-C. ^{b} See Supporting Information.

(**16** to **17**) is exothermic by 3.1 kcal/mol, the dihydrogen activation in a Ni(III) state is thermodynamically favorable over that in either the Ni(I) or Ni(II) states. For all Ni(III) species, **16**, **17**, and **20**, the CO distances are shorter than that of **1**, our candidate for **Ni-B**. Since the experimental IR spectra shows that the **Ni-C** species has a slightly higher vibrational frequency ($+6$ cm^{-1}) than the **Ni-B** state, the most likely candidate for the **Ni-C** species is **20** because it has a slightly shorter CO distance (-0.006 Å) than **1**, whereas **17** has a much shorter CO distance. The optimized geometry of **20** shows that the hydride ligand occupies a metal bridging site (bridging geometries are higher in energy) that is an equatorial (in-plane) Ni site. The experimental (EPR) g values for the **Ni-C** signal ($g_x \neq g_y > g_z \approx 2$) indicate that its unpaired electron occupies the d_{z^2} orbital of a nickel with a rhombically distorted octahedral symmetry.[3e,21] The ENDOR shows a large hyperfine coupling ($A^H(1) = 16.8$ MHz) on the exchangeable proton,[21] which suggest a direct interaction between H and Ni, but rules out a hydride bound axially to the **Ni-C**. The other proton is separated from the Ni by an additional atom.[21] The calculated geometrical features of **20** are in good agreement with the IR, EPR, and ENDOR results. All of the evidence points to the hydride bridging complex **20** as the **Ni-C** species.

Compared to the Ni(III) species, **20**, the Ni(I) isomer **19** is more stable by 11 kcal/mol. Thus, the conversion from **20** to **19** is thermodynamically favorable. Although **19** is potentially observable, the final electron and proton transfer to reform **Ni-SI** (**19** → **Ni-SI(b)** + H$^+$ + e$^-$) may be faster than the formation of **19** from **20** (**19** → **20**). Thus, **19** would not be observed in the usual experiments. However, **19** or a closely related species could be a candidate for a Ni-L form as it would lack the H hyperfine found in **Ni-C** and would have a relatively high ν_{CO}.[3c]

Redox Species in the Active Site of the Catalytic Cycle. To confirm the internal consistency of our proposed assignment for the redox states of the active site, we have made a correlation between their calculated CO distances and the natural logarithm of their observed vibrational frequencies[3g−h] in Figure 8, which shows a very good correlation (correlation coefficient = 0.905). In comparison to the organometallic model complexes (Figure 1), the slope in Figure 8 is less because the greater total electron density in the [NiFe] hydrogenase model weakens the CO response.[22] Table 1 summarizes the influence of redox and protonation of the [NiFe] hydrogenase model on the CO bond by tabulating the predicted CO distances of all calculated species as a function of redox and protonation state. One finds the expected trends: (i) as protons are added, the CO bond distance gets shorter and (ii) as electrons are added, the CO bond distance gets longer. Thus, the IR band shifts in the active site of the enzyme reflect the changes in the valence state and the coordination environment of the Ni center. Overall, there is an excellent correlation between the CO distances of all the

(21) Fan, C.-L.; Teixeira, M.; Moura, J.; Moura, I.; Hutnh, B.-H.; Gall, J. L.; Peck, H. D.; Hoffman, B. M. *J. Am. Chem. Soc.* **1991**, *113*, 20.
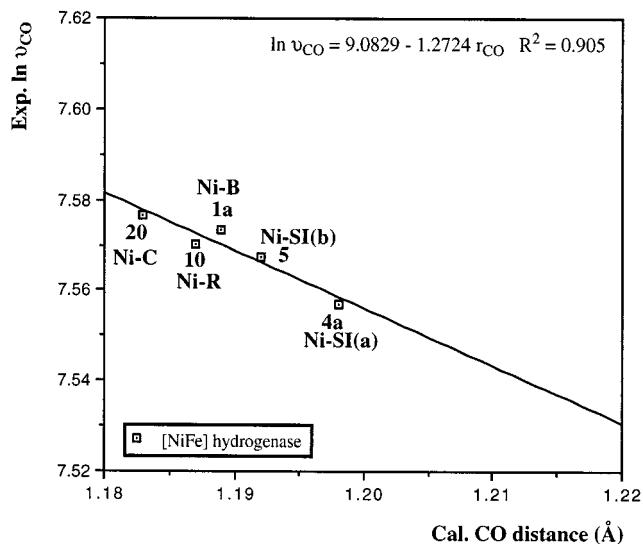
(22) For example, we have obtained an excellent linear correlation for r_{CO} vs ln ν_{CO} for the transition-metal monocarbonyl complexes, M−CO (M = Fe, Co$^+$, Ni^{2+}, Ru, Rh$^+$, Pd^{2+}), where the correlation coefficent is 0.981. The slope here is 2.61, which is 35% greater than that obtained for the organometallic system LFe(CO)(CN)(L′)$^{n-}$. Thus, the 34% decrease in slope for the enzyme system with respect to the organometallic system LFe(CO)(CN)(L′)$^{n-}$ is quite reasonable.

(23) Mulliken, R. S. *J. Chem. Phys.* **1955**, *23*, 1833, 1841, 2338, 2343.

Nickel−Iron Hydrogenase of Desulfovibrio gigas

J. Am. Chem. Soc., Vol. 121, No. 16, 1999 4007

Table 2. the Calculated Mulliken Charge Density (e)[a] at the Ni and Fe Centers for the Proposed Active Site Species of [NiFe] *D. gigas* Hydrogenase

	Ni	Fe
Ni-B	−0.705	−1.206
Ni-SI(a)	−0.642	−1.296
Ni-SI(b)	−0.745	−1.505
Ni-R	−0.753	−1.842
Ni-C	−0.638	−1.927

[a] The Mulliken charges are not accurate in an absolute sense, but should correctly reflect the trends as these closely related species change oxidation state and coordination.[23]

Scheme 6
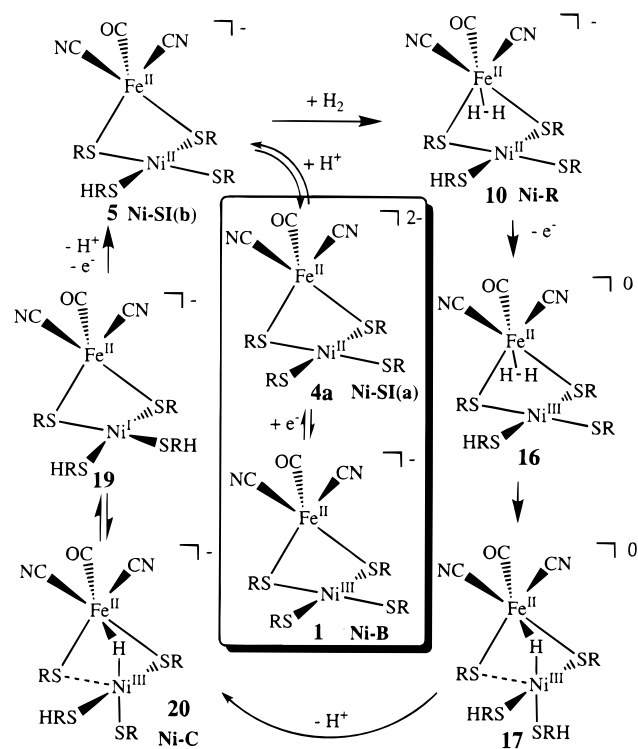
proposed structures and the IR data of the hydrogenase active site species.[3g−h] In addition, we have investigated the electron density of the proposed redox states of the active site for [NiFe] *D. gigas* hydrogenase (see Table 2). The calculated Mulliken charges show that the electron density at Ni from the "ready" state **Ni-B** (Ni(III)) through the **Ni-SI** (Ni(II)) and **Ni-R** (Ni-(II)) species to the **Ni-C** (Ni(III)) species is relatively constant (from −0.64 to −0.75 e) despite the different formal oxidation states. This result is consistent with the X-ray absorption edge results,[3i] where no significant change in electron density at the Ni center is observed during **Ni-SI** → **Ni-R** → **Ni-C** transformations.

Accordingly, our proposed structural cycle for [NiFe] *D. gigas* hydrogenase is shown in Scheme 6. First, partial reduction of the enzyme in the **Ni-B** form, **1**, yields the **Ni-SI(a)** species, **4a**, which is followed by protonation at a terminal cysteine to generate the **Ni-SI(b)** species, **5**. Then, the **Ni-SI(b)** species, **5**, reacting with H_2 generates the **Ni-R** species, **10**, which has an η^2-H_2 bound to Fe. Electron transfer (oxidation) occurs to form the Ni(III) species **16** which then rapidly activates H_2 to form **17**, which has a Ni−H−Fe bridged framework, followed by proton transfer from a terminal cysteine to form the **Ni-C** species, **20**. The hydride rearrangement in **20** leads to a Ni(I) species, **19**, which returns to the **Ni-SI(b)** species, **5**, by electron (oxidation) and proton transfers; a second proton transfer results

in the formation of the **Ni-SI(a)** species, **4a**. Thus, the **5** (**Ni-SI(b)**), **10** (**Ni-R**), **16**, **17**, **19**, and **20** (**Ni-C**) forms participate in the catalytic cycle of the [NiFe] hydrogenase, whereas the **1a** (**Ni-B**) and **4a** (**Ni-SI(a)**) species are involved in the activation process.

Conclusions

By combining the spectroscopic results with the computational results on the [NiFe] *D. gigas* hydrogenase model and the organometallic complexes, LFe(CO)(CN)(L′)$^{n-}$ (L = Cp or Cp*, L′ = CN, CO, CNCH₃; $n = 0, 1, 2$), the intermediate species (**Ni-B, Ni-SI(a), Ni-SI(b), Ni-R**, and **Ni-C**) have been identified and their structures determined. Our final set of proposed structures for the cycle, as shown in Scheme 6, are consistent with IR, EPR, ENDOR, and XAS measurements for these species.

From our calculations it would appear that the tendency of the Fe(μ-S)₂Ni framework to fold and unfold upon protonation may play an important role in H_2 activation. This folding is driven by protonation of a terminal sulfur, which decreases its covalent bonding to Ni, and Ni, in turn, increases its covalent bonding to the bridging sulfur, which causes a decrease of about 18° in the Fe−S−Ni angle(s). Since the energy differences between the folded and unfolded structures are small, the protein backbone may contribute significantly to this aspect of the structure and mechanism. Although the idea is not generally accepted, the calculations strongly suggest that the Fe center is the site of the initial capture of the dihydrogen. The low-spin d⁶ Fe with the soft donor and π acceptor ligands is especially well suited for this role.[24] Also unexpected is the high oxidation state needed on Ni (Ni(III)) prior to H_2 bond activation. One might expect H_2 activation to be easier on lower oxidation state Ni, but it is not. For Ni(II) species, the four-coordinate complex **10** is stable so the activation of H_2 is endothermic. However, after oxidation, the Ni(III) species, **16,** is relatively unstable but formation of a new Ni−H bond in **17** stabilizes the Ni(III) species. Thus, H_2 activation is only exothermic for the Ni(III) species. The calculations show that the proton transfer from the bridging site of **20** to the terminal cysteine yields isomer, **19**. These new intermediates, **16**, **17**, and **19**, proposed in our cycle may all be relatively short-lived and may, as yet, be unobserved.

These results provide significant insight into the structural changes taking place at the active site in the catalytic cycle of the [NiFe] hydrogenase. Having established the nature of the thermodynamically "stable" intermediates observed experimentally, one can begin to search for kinetically viable transition states between them. Further work will also involve adding the protein backbone as it may play an essential role in the folding and, hence, the Ni−Fe distance of the [NiFe] hydrogenase.

Supporting Information Available: The B3LYP optimized geometries of some Ni(I) species, **21**, **22**, and **23**, and a Ni(0) species **24** (PDF). This material is available free of charge via the Internet at http://pubs.acs.org.

JA983469R

(24) A suggestion also made by S. Koch, 5th International Conference on Mol. Bio. Hydrogenase, July 1997.